Annals of Nuclear Medicine Vol. 15, No. 2, 123–129, 2001

Brain perfusion SPECT study with ^{99m}Tc-bicisate: Clinical pitfalls and improved diagnostic accuracy with a combination of linearization and scatter-attenuation correction

Hirotsugu KADO,* Hidehiro IIDA,** Hirohiko KIMURA,* Toshihide OGAWA,** Yuichiro NARITA,** Jun HATAZAWA,** Tatsuro TSUCHIDA,* Yoshiharu YONEKURA*** and Harumi ITOH*

Department of Radiology, Fukui Medical University
**Department of Radiology and Nuclear Medicine, Akita Research Institute of Brain and Blood Vessels*
***Biomedical Imaging Research Center, Fukui Medical University*

To evaluate the usefulness of a combination of linearization and scatter-attenuation correction on ^{99m}Tc-bicisate (ECD)-single photon emission tomographic (SPECT) images, both cerebral blood flow (CBF)-positron emission tomographic (PET) images and ECD-SPECT images from fifteen patients with chronic cerebral infarction were acquired. We measured radioactivity counts in regions of interest (ROIs) on all sets of both images and obtained a 2D scattered graph between ECD-SPECT and CBF-PET data. To evaluate diagnostic accuracy, the sensitivity, specificity and accuracy of ECD-SPECT images were calculated by means of discriminant analysis. The same analysis was also performed on the ECD-SPECT images corrected by a combination of linearization and scatter-attenuation correction. An overall nonlinear relationship was observed between ECD-SPECT and CBF-PET. The sensitivity, specificity, and accuracy of ECD-SPECT images were 69.6%, 91.4% and 73.0%, and those of ECD images corrected by the combination of linearization and scatter-attenuation correction were 79.5%, 95.7% and 82.0% respectively. The clinically diagnostic accuracy of ECD-SPECT images corrected by the combined method apparently increased. So that the linearization with the scatter-attenuation method is useful for improving the diagnostic accuracy of ECD-SPECT images.

Key words: ^{99m}Tc-bicisate (ECD)-SPECT, CBF-PET, linearization, scatter-attenuation correction.

INTRODUCTION

^{99m}Tc-bicisate (Daiichi Radioisotope Laboratories, Tokyo, Japan; ECD) is a brain-retained tracer for single photon emission computed tomography (SPECT), and its distribution is considered to reflect regional cerebral blood flow (rCBF) in the human brain.[1,2] Nevertheless, the relatively low first-pass extraction of this tracer into the brain tissue has been shown to cause a nonlinear relationship between ECD uptake and rCBF as measured by positron emission tomography (PET).[3] It is, therefore, hypothesized that the diagnostic accuracy of ECD-SPECT images may be limited. Based on a comparison of ECD-SPECT and CBF-PET images, we assessed the effect of three ECD-SPECT images on clinical diagnosis. One was the effect of ECD-SPECT images without any correction, one was that of ECD-SPECT images with linearization based on a permeability-surface area product (PS) model,[4–7] and one was that of ECD-SPECT images with the combination of linearization and scatter-attenuation correction. Our goals were to assess the clinical pitfalls and to evaluate by means of discriminant analysis the usefulness of the combination of linearization and scatter-attenuation correction on ECD-SPECT images.

Received September 5, 2000, revision accepted January 24, 2001.

For reprint contact: Hirotsugu Kado, M.D., Department of Radiology, Fukui Medical University, 23 Shimoaizuki, Matsuoka-cho, Yoshida-gun, Fukui 910–1193, JAPAN.
E-mail: kado@fmsrsa.fukui-med.ac.jp

MATERIALS AND METHODS

Subjects

Fifteen patients with chronic cerebrovascular disease participated in this study (ages ranged from 47 to 77; mean 63.2 ± 7.9 years old). Subjects are summarized in Table 1. All subjects gave written informed consent to the study protocol, which had been approved by the committee for clinical research of this institute.

PET measurement

The PET machine used was a Headtome IV (Shimadzu Corp., Kyoto, Japan), a four-ring, seven-slice scanner.[8] With axial continuous motion of the gantry, this scanner provides 14 tomographic slices simultaneously. The intrinsic resolution was 4.5 mm full-width at half maximum (FWHM) in-plane, and 9.5 mm FWHM axially. CBF was measured by the steady-state method. After the patient continuously inhaled (^{15}O)CO_2, PET recording continued in the steady-state condition for 10 min. Three arterial blood samples were obtained from the radial artery, and their radioactivity concentrations were counted in a well counter cross-calibrated to the PET scanner. The acquired tomographic slices were parallel to the orbito-meatal (OM) line.

The steady-state technique was employed for quantitation of CBF with (^{15}O)CO_2 and PET. In the model calculation, the tissue/blood partition coefficient of water and the extraction fraction of water were assumed to be constant. The CBF was then calculated as:

$$f = \lambda/(C_a/C_t - 1/p), \quad (1)$$

where f denotes CBF (ml/min/100 g), C_a is the arterial radioactivity, and C_t is the regional brain tissue radioactivity in the steady-state condition. λ represents the radioactive decay constant for ^{15}O. p is the tissue/blood partition coefficient of water.

^{99m}Tc-bicisate

A ^{99m}Tc-bicisate kit (Daiichi Radioisotope Laboratories, Tokyo, Japan) comprised two vials, A and B. Vial A contained sterile and nonpyrogenic freeze-dried bicisate, and Vial B contained a liquid form of phosphate buffer. Normal saline (3.0 m*l*) was injected into Vial A to dissolve its contents. Two m*l* of 1110 MBq (30 mCi) of ^{99m}Tc generator eluate was injected into Vial B. Then 1.0 m*l* was transferred from Vial A to Vial B. The mixture was allowed to stand at room temperature for at least 15 min. The radiochemical purity of the final solution was determined by thin layer chromatography. The labeling efficiency of this ^{99m}Tc-bicisate was about 97%.

SPECT measurement

After the PET study, a SPECT study with a ^{99m}Tc-bicisate (ECD-SPECT) was carried out within an interval of less than 1 hour in each patient. Approximately 740 MBq (20 mCi) of ^{99m}Tc-bicisate was injected intravenously into each subject. The ECD-SPECT imaging was performed from 5 to 30 min after the administration of the agent with a ring-type SPECT scanner (Headtome-II; Shimadzu Corp., Kyoto, Japan). The SPECT machine had three detector rings with 64 NaI rectangular detectors,[9] the spatial resolution at the center of the field of view (FOV) was 8 mm FWHM, and the slice thickness was 17 mm. The acquired tomographic slices were parallel to the orbito-meatal (OM) line. The images were reconstructed by filtered backprojection with a Butterworth filter. Attenuation correction was done by elliptical fitting.

Table 1 The patients with chronic cerebrovascular disease are summarized

No.	sex	age (y.o.)	CT/MRI diagnosis and other findings	time from onset
1	M	70	large infarction in lt ICA territory, lt ICA occlusion	18 months
2	M	68	large infarction in rt MCA territory, rt MCA stenosis (95%)	12 months
3	F	68	large infarction in rt MCA territory, rt MCA occlusion	8 months
4	M	64	large infarction in rt ACA territory, rt ACA occlusion	10 months
5	M	51	lacunar infarction in lt BG, multiple spotty LDAs in lt BG	6 months
6	F	69	large infarction in rt MCA territory, rt MCA stenosis (90%)	15 months
7	M	77	lacunar infarction in rt BG, spotty LDA in rt BG	7 months
8	M	57	lacunar infarction in rt BG, multiple spotty LDAs in rt BG	9 months
9	M	67	large infarction in lt MCA territory, lt MCA occlusion	8 months
10	M	67	lacunar infarction in rt BG, multiple spotty LDAs in rt BG	5 months
11	F	63	large infarction in rt ACA territory, rt ACA occlusion	9 months
12	M	54	large infarction in lt MCA territory, lt MCA occlusion	16 months
13	M	65	large infarction in lt MCA territory, lt MCA occlusion	21 months
14	F	61	lacunar infarction in lt BG, spotty LDA in lt BG	5 months
15	M	47	large infarction in lt ACA territory, lt ACA stenosis (99%)	9 months

ICA: internal carotid artery, ACA: anterior cerebral artery, MCA: middle cerebral artery, BG: basal ganglia, lt: left, rt: right

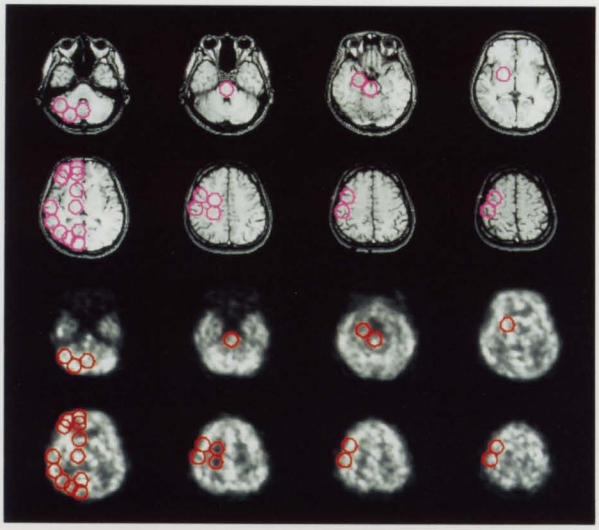

Fig. 1 Regions-of-interest (ROIs) selected in this study: 1) the pons, 2) the mid brain, 3) the cerebellar vermis, 4) the cerebellar hemisphere, 5) the caudate nucleus, 6) the lentiform nucleus, 7) the thalamus, 8) the hippocampal gyrus, 9,10,11) the superior, middle, and inferior temporal gyri, 12) the cingulate gyrus, 13, 14,15) the superior, middle, and inferior frontal gyri, 16,17) the precentral and postcentral gyri, 18) the occipital ceneus, 19,20) the posterior and lateral areas of the occipital lobe, and 21) the centrum semiovale. Regions are shown in only one hemisphere, though ROIs were duplicated in the other one.

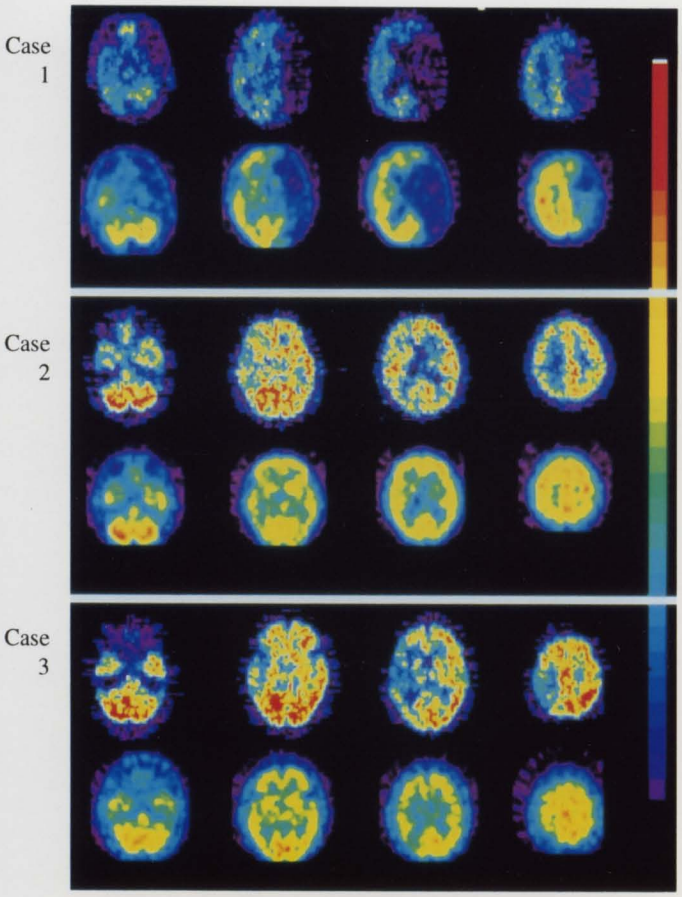

Fig. 2a Examples of comparisons among these cases of ECD uptake (lower row) and rCBF assessed by PET with (^{15}O)CO_2 (upper row).

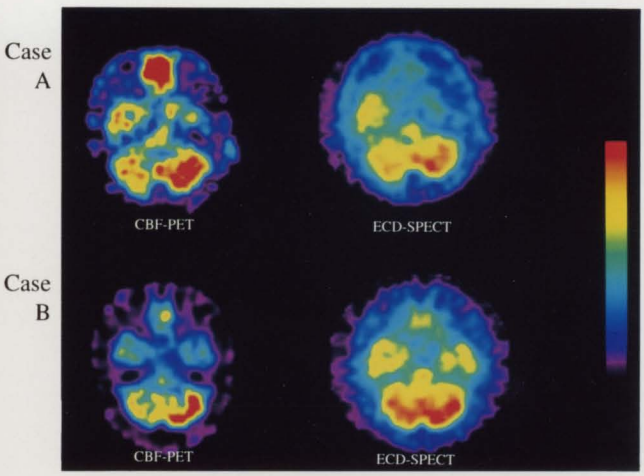

Fig. 2b Examples of comparisons between two cases of ECD uptake and CBF-PET image in cerebellar radioactivity concentrations.

Linearization of ECD uptake

Assuming that the ECD uptake follows the PS model, the linearization[7] was performed on the ECD-SPECT images as follows:

$$C/Cr = F/Fr \times (1 - \exp(-PS/F))/(1 - \exp(-PS/Fr)), \quad (2)$$

where F is rCBF (ml/min/100 g). F/Fr is the rCBF value ratio in the reference region. C/Cr is the relative SPECT count. This equation can be simplified as

$$Y = X(1 - Z^{(1/X)})/(1 - Z), \quad (3)$$

where X = F/Fr, Y = C/Cr, and Z = exp(–PS/Fr).

The relation between the relative ECD uptake (C/Cr) and the relative rCBF measured by PET (F/Fr) was first fitted to the equation, then from the look-up table, Y was

calculated for each X value, and the relationship of X to Y was obtained by fourth-order polynominal curve fitting.[7]

Scatter correction

The triple energy window (TEW) technique uses two small (3%) subwindows, just below and above the main photo peak window (24% centered on 140 keV).[12] The scatter estimate for the main window is then given the weighted average of the counts in the subwindows.

Three scattered plots graphs between rCBF and ECD uptake

To obtain three 2D scattered plots graphs, we compared rCBF values and the corresponding ECD uptake of three ECD-SPECT images. One was the comparison of CBF-PET images and ECD-SPECT images without any correction (ECD^1-SPECT), one was that of CBF-PET images and ECD-SPECT images with linearization (ECD^2-SPECT), and one was that of CBF-PET images and ECD-SPECT images corrected by the combination of linearization and scatter-attenuation correction (ECD^3-SPECT).

Before the comparison of PET images and the three ECD-SPECT (ECD^1-SPECT, ECD^2-SPECT and ECD^3-SPECT) images, the CBF-PET and three ECD-SPECT images were registered with the MR images of the corresponding subject by using the software of a fully automatic multimodality registration algorithm[10] (Department of Radiology and Nuclear Medicine, Akita Research Institute of Brain and Blood Vessels, Akita, Japan).

After the registration, a total of 51 regions of interest (ROIs) were drawn on both hemispheres on the MRI images, then superimposed onto the registered CBF-PET and three ECD-SPECT images. The criteria[11] for ROI selection are shown in Figure 1. All ROIs were circular and approximately 24 mm in diameter. We used the mean values in the cerebellar hemisphere, the centrum semiovale, the precentral gyrus, and the postcentral gyrus. Therefore, a total of 39 ROIs were selected for a scattered plots graph in each image.

The rCBF values were normalized as the % ratio of ROI counts relative to the counts in the ipsilateral cerebellum region (F/Fr). The reason why we selected the counts in the ipsilateral cerebellum region was to exclude the effects of crossed-cerebellar diaschisis (CCD). We performed the same normalization of the relative ECD uptake (C/Cr) on the three ECD-SPECT (ECD^1-SPECT, ECD^2-SPECT and ECD^3-SPECT) images and evaluated the C/Cr in ECD^1-SPECT images (C^1/Cr), the C/Cr in ECD^2-SPECT images (C^2/Cr), and the C/Cr in ECD^3-SPECT images (C^3/Cr).

We then compared F/Fr and C^1/Cr, and obtained their relationship on a 2D scattered plots graph ($graph^1$) in order to apply discriminant analysis. After that, the same comparison was performed to obtain a plots graph for F/Fr and C^2/Cr ($graph^2$). This was performed a third time for F/Fr and C^3/Cr ($graph^3$).

Discriminant analysis

To determine which correction methods could improve the diagnostic accuracy of ECD-SPECT images clinically, we examined the sensitivity, specificity, and accuracy of the three ECD-SPECT (ECD^1-SPECT, ECD^2-SPECT and ECD^3-SPECT) images of the corresponding subject. We assumed the relative rCBF values to be true, and a linear discriminant analysis (Release 6.0; SPSS, Chicago, III) was applied with three 2D scattered plots graphs ($graph^1$, $graph^2$ and $graph^3$). We defined the value of 0.8 in F/Fr as the threshold of mild hypoperfusion. A value of 0.8 in F/Fr was defined as −2SD of the mean relative cerebellar blood flow (CeBF) value in the CCD-affected area (0.850 ± 0.025 in F/Fr). The reason why the threshold of mild hypoperfusion was defined with the CeBF values in the CCD-affected area (CCD-CeBF) was that the reduced CCD-CeBF never caused infarction or cerebellar dysfunction. Therefore, we thought that the flow values would be suitable to define the threshold of mild hypoperfusion. By means of discriminant analysis with a $graph^1$, we evaluated the sensitivity, specificity, and accuracy of ECD^1-SPECT in that flow range. After that, in order to examine the effect of the other correction methods, a similar discriminant analysis was applied with $graph^2$ and $graph^3$ in the same flow range.

RESULTS

Figure 2-a shows examples of comparisons of the ECD uptake with rCBF images assessed by PET and $(^{15}O)CO_2$ in three cases. In case 1 (patient number 1), both ECD uptake and CBF images were diffusely decreased, showing relatively good agreement with each other. In case 2 (patient number 2), a small defect in the right frontal lobe was observed on CBF-PET, which partially agrees with the area of severe hypoperfusion on ECD-SPECT. In case 3 (patient number 3), the hypoperfused area on ECD-SPECT was underestimated in comparison with that on CBF-PET. Mismatch between the ECD-SPECT and CBF-PET images was observed in areas that showed relatively mild hypoperfusion.

Figure 2-b shows examples of comparisons of the ECD-SPECT and CBF-PET images in terms of cerebellar radioactivity concentrations. The reduction of cerebellar blood flow (CeBF) due to CCD is seen in both cases. In case A (patient number 1), ECD uptake in the right cerebellum (CCD-affected side) was visually in good agreement with the ipsilateral CeBF on the PET images. In case B (patient number 5), the differences between the right (CCD-affected side) and left cerebellum (CCD-unaffected side) could not be observed clearly on the ECD-SPECT image, but the differences were clear on the CBF-PET image.

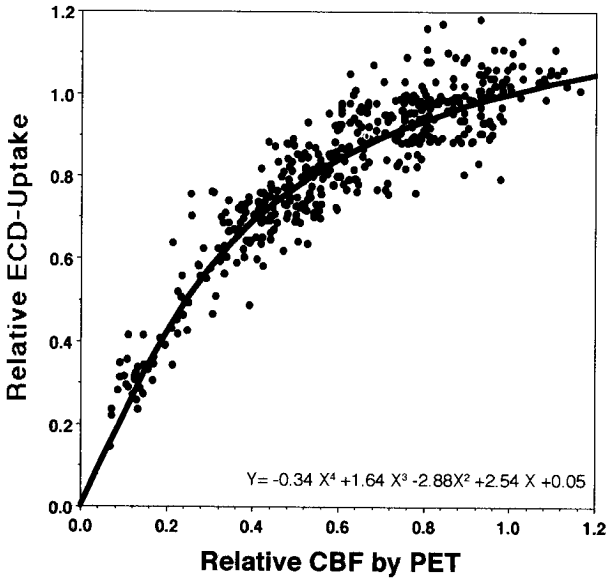

Fig. 3 The relationship between the relative ECD[1] uptake and relative CBF by PET. The values were calculated as relative to the CCD-unaffected cerebellum.

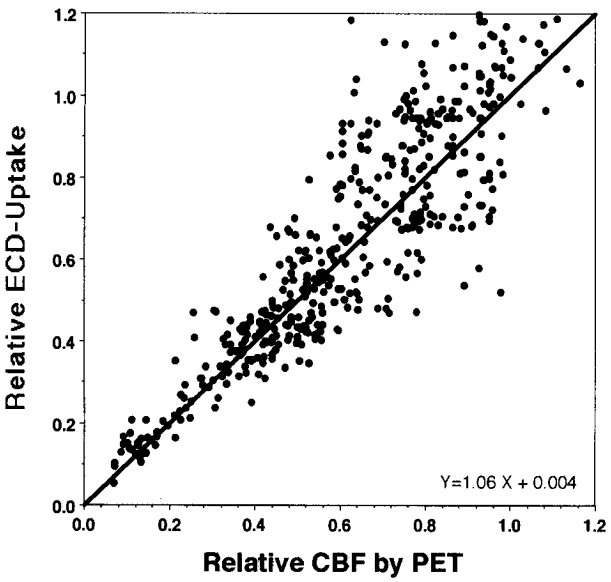

Fig. 4 The relationship between the relative ECD[2] uptake (linearized ECD uptake based on the PS model) and relative CBF by PET. The values were calculated as relative to the CCD-unaffected cerebellum.

The overall nonlinear relationship between C[1]/Cr and F/Fr is shown in Figure 3 (graph[1]). The ECD[1]-SPECT counts were saturated but gradually increased at a flow range of more than about 0.6 in F/Fr. The mean value for relative CeBF in the CCD-affected area was 0.850 ± 0.025 in F/Fr.

Figure 4 shows the relationship between C[2]/Cr and F/Fr (graph[2]). Despite good linearity obtained by the linearization procedure, the correction increased the distances

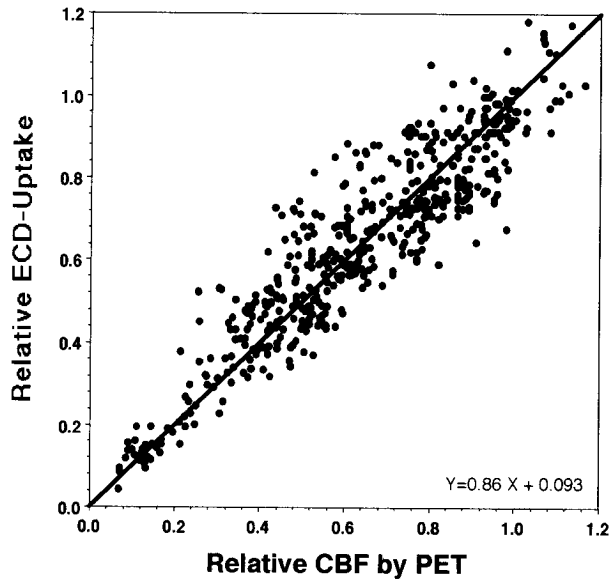

Fig. 5 The relationship between the relative ECD[3] uptake (linearized ECD uptake with the scatter-attenuation correction method) and relative CBF by PET. The values were calculated as relative to the CCD-unaffected cerebellum.

of the scattered dots from the regression line, particularly within a range of more than mild hypoperfusion (≥ 0.8 in F/Fr).

Figure 5 shows the relationship between C[3]/Cr and F/Fr (graph[3]). In addition to good linearity obtained by the linearization procedure, the distances of scattered dots from the regression line was improved within a range of more than mild hypoperfusion (≥ 0.8 in F/Fr).

There were three ECD[3]-SPECT images in which we thought that the differences between the CCD-affected side and CCD-unaffected side could be clarified in comparison with that on ECD[1]-SPECT. In two ECD[3]-SPECT images, the underestimated areas of hypoperfusion (ischemia) were thought to be improved compared to the CBF-PET images.

When 0.8 in F/Fr on PET data was used as the threshold of mild hypoperfusion, the sensitivity, specificity, and accuracy of ECD[1]-SPECT, ECD[2]-SPECT and ECD[3]-SPECT were 69.6%, 91.4% and 73.0% on ECD[1]-SPECT, 78.3%, 81.7% and 78.8% on ECD[2]-SPECT, and 79.5%, 95.7% and 82.0% on ECD[3]-SPECT, respectively. The linearization procedure did not improve the diagnostic accuracy, but the combination of linearization and the scatter-attenuation correction method did increase the diagnostic accuracy.

DISCUSSION

ECD uptake images were used as an rCBF map *in vivo* by using SPECT but it was demonstrated that ECD accumulation has a nonlinear relationship with the true rCBF, which is of some importance in clinical interpretation. In

this context, the mildly hypoperfused area and the CCD phenomenon may be underestimated or neglected on ECD-SPECT images.

There are several reasons for the nonlinear accumulation of ECD. From the perspective of pharmacokinetics, a major factor is probably limited extraction. That is due to the relatively small permeability-surface (PS) area product.[6,7] In addition to the rapid blood clearance, ECD shows rapid conversion from the original lipophilic compound to hydrophilic metabolites in brain tissue and blood.[2] Therefore, arterial input to the brain tissue is limited within the short period after intravenous injection. Limited extraction reduces the radioactivity counts on the SPECT machine, particularly in a high-flow region. A washout of ECD[13] from the brain into the venous drainage is also believed to be a factor in the nonlinear relationship. That may limit the retention of ECD in the interstitial spaces in brain tissue. The hypofixation of ECD in the subacute phase, which could reduce the radioactivity counts relative to the true rCBF, has been reported,[14] but the stage of infarction in all cases was chronic. We therefore think that the effect of hypofixation of ECD did not contribute to the nonlinear relationship in this study.

From a physical perspective, the scatter and attenuation photons on SPECT images were also considered to be an important factor, because they may have caused the lower contrast and nonlinearity. New scatter and attenuation correction methods[12,15] have recently been developed, and the contrast and linearity on SPECT images have thus been improved, though not completely eradicated. Lower spatial resolution on both the transaxial plane and in the axial direction on the SPECT machine causes a loss in the counts, which is a factor contributing to the nonlinear relationship. Unfortunately, we could not find effective methods of dealing with these problems in lower spatial resolution on SPECT.

Although the linearization procedure did improve the contrast and linearity, this investigation also demonstrated that the simple application of linearization based on the PS model did not sufficiently improve accuracy. This is because linearization enchances the distance of scattered dots from the straight line (or regression line). The relative values, which fit on the curved line based on the PS model, are replaced on the straight line (or regression line) by the linearization procedure. But the other relative values, which are scattered far from the curved line, augment its distance from the straight line (or regression line) by the linearization procedure. Therefore, before applying the linearization procedure, it is necessary that the nonlinearity be improved and the contrast is increased, though not completely eradicated.

The scatter-attenuation correction is considered an effective method of improving the contrast and the overall nonlinearity of SPECT, though it does not completely eradicate these problems. Iida et al. reported that proper scatter-attenuation correction could improve noise, contrast and the nonlinear relationship between SPECT and PET images.[15] They were successful in increasing the gray-to-white ratio until it was close to that of the PET measurement with that correction. In our study, the scatter-attenuation correction method could also improve the image contrast and the overall nonlinearity before linearization. In addition, the relative values, which did not fit on the curved line, did not augment its distance from the straight line (or regression line) by the linearization procedure. We therefore think that the combination of linearization and scatter-attenuation correction was successful in increasing the clinical accuracy of ECD-SPECT images. Our data showed the usefulness of ECD^3-SPECT images. How to optimize the scatter-attenuation correction method, however, remains to be investigated.

Although important and interesting findings on ECD-SPECT images are often underestimated at a flow range of more than about 0.6 in F/Fr, we think that the clinical usefulness of ECD-SPECT is not so limited. This is because it is most important to know what happens in a patient's brain and to decide what clinical diagnosis should be made based on the information gathered from ECD-SPECT images. Actually, in most cases, the patients who need to go through a CBF examination often have a transient ischemic attack (TIA), ischemia, atrophy, infarction, depression, and dementia in many hospitals. Many of them have diseases that cause reduced rCBF. ECD can precisely estimate rCBF in that low-flow range. Therefore, it is valuable to try to detect where abnormal rCBF is distributed in many cerebrovascular diseases. On the other hand, ECD does not reflect luxury perfusion in the early recanalization stage of infarction. It is also useful in diagnosing this phenomenon as an infarction at that stage, compared to the other CBF tracers such as ^{99m}Tc-HMPAO, ^{123}I-IMP, (^{15}O)CO_2 and (^{15}O)H_2O. These tracers reflect luxury perfusion and are accumulated even in the infarcted area after early recanalization. Even if we want to find a hyperperfused brain disease such as epilepsy, ECD is thought to be useful. This is because the ECD uptake tends to increase gradually at a flow range of more than about 0.6 in F/Fr, while keeping the overall nonlinear relationship. Although the increased rCBF values in the focus cannot be estimated exactly, the information from ECD is enough to diagnose epilepsy and to detect the position of the focus clinically. But we believe that precise investigations with ECD-SPECT images, such as the detection of CCD phenomenon, the exact area of ischemia, the exact evaluation of the cerebrovasodilative capacity by diamox activation, and the quantitation of rCBF with ECD-SPECT may be limited. As mentioned above, ECD is useful in most clinical cases, but the usage of ECD for precise study and examination is restricted. We should pay careful attention to detailed investigations the range of more than mild hypoperfusion.

CONCLUSIONS

Although ECD-SPECT images are used to visualize brain perfusion in patients with cerebrovascular disorders, the nonlinear relationship between ECD uptake and true rCBF could cause or contribute to misinterpretation. A linearization procedure without the scatter-attenuation correction can increase contrast but cannot improve the diagnostic accuracy of ECD-SPECT images. A linearization procedure with scatter-attenuation correction could improve the diagnostic accuracy. To achieve better accuracy of ECD-SPECT images clinically, the optimization of the combined linearization with scatter-attenuation correction method should be studied further.

REFERENCES

1. Kung HF, Guo YZ, Yu CC, Billings J, Subramanyam V, Calabrese JC. New brain perfusion imaging agents based on Tc-99m bis-(aminoethanethiol) complexes: stereoisomers and biodistribution. *J Med Chem* 1989; 32: 433–437.
2. Walovitch RC, Hill TC, Garrity ST, Cheesman EH, Burgess BA, O'Leary DH, et al. Characterization of technetium-99m-L,L-ECD for brain perfusion imaging, part 1: pharmacology of technetium-99m ECD in nonhuman primates. *J Nucl Med* 1989; 30: 1892–1901.
3. Kundsen GM, Andersen AR, Somnier FE, Videbaek C, Hasselbalch S, Paulson OB. Brain extraction and distribution of Tc-99m bicisate in humans and in rats. *J Cereb Blood Flow Metab* 1994; 14 (Suppl 1): S12–S18.
4. Crone C. The permeability of capillaries in various organs as determined by use of the "indicator diffusion" method. *Acta Physiol Scand* 1963; 58: 292–305.
5. Raichle ME, Eichling JO, Straatmann MG, Welch MJ, Larson KB, Ter-Pogossian MM. Blood-brain barrier permeability of C-11-labeled alcohols and O-15-labeled water. *Am J Physiol* 1976; 230: 543–552.
6. Yonekura Y, Tsuchida T, Sadato N, Nishizawa S, Iwasaki Y, Mukai T, et al. Brain perfusion SPECT with Tc-99m-bicisate: comparison with PET measurement and linearization based on permeability-surface area product model. *J Cereb Blood Flow Metab* 1994; 14 (Suppl 1): S58–S65.
7. Tsuchida T, Yonekura Y, Nishizawa S, Sadato N, Tamaki N, Fujita T, et al. Nonlinearity correction of brain perfusion SPECT based on permeability-surface area product model. *J Nucl Med* 1996; 37: 1237–1241.
8. Iida H, Miura S, Kanno I, Murakami M, Takahashi K, Uemura K, et al. Design and evaluation of Headtome 4, a whole-body positron emission tomograph. *IEEE Trans Nucl Sci* 1989; 36: 1006–1010.
9. Kanno I, Uemura K, Miura S, Miura Y. Headtome: A hybrid emission tomograph for single photon and positron emission imaging of the brain. *J Comput Assist Tomogr* 1981; 5: 216–226.
10. Ardekani BA, Braun M, Hutton BF, Kanno I, Iida H. A fully automatic multimodality image registration algorithm. *J Comput Assist Tomogr* 1995; 19: 615–623.
11. Yamaguchi T, Kanno I, Uemura K, Shishido F, Inugami A, Ogawa T, et al. Reduction in regional cerebral metabolic rate of oxygen during human aging. *Stroke* 1986; 17: 1220–1228.
12. Ogawa K, Ichihara T, Kubo A. Accurate scatter correction in single photon emission CT. *Ann Nucl Med* 1994; 7: 145–150.
13. Lars F, Allan RA, Niels AL, Søren H, Mogens D. Retention of Tc-99m bicisate in the human brain after intracarotid injection. *J Cereb Blood Flow Metab* 1994; 14: S19–S27.
14. Lassen NA, Sperling B. ^{99m}Tc-bicisate relatively images CBF in chronic brain diseases but fails to show reflow hyperemia in subacute stroke: report of a multicenter trail of 105 cases comparing ^{133}Xe and ^{99m}Tc-bicisate (ECD, neurolite) measured by SPECT on same day. *J Cereb Blood Flow Metab* 1994; 14: S44–S48.
15. Iida H, Narita Y, Kado H, Kashikura A, Sugawara S, Shoji Y, et al. Effects of scatter and attenuation correction on quantitative assessment of regional cerebral blood flow with SPECT. *J Nucl Med* 1998; 39: 181–189.